In Vivo PET Imaging of the Cancer Integrin αvβ6 Using ^{68}Ga-Labeled Cyclic RGD Nonapeptides

Johannes Notni[1], Dominik Reich[1], Oleg V. Maltsev[2], Tobias G. Kapp[2], Katja Steiger[3], Frauke Hoffmann[1], Irene Esposito[4], Wilko Weichert[3], Horst Kessler[2], and Hans-Jürgen Wester[1]

[1]Lehrstuhl für Pharmazeutische Radiochemie, Technische Universität München, Garching, Germany; [2]Institute for Advanced Study and Center of Integrated Protein Science (CIPSM), Department Chemie, Technische Universität München, Munich, Germany; [3]Institute of Pathology, Technische Universität München, Munich, Germany; and [4]Institute of Pathology, Universitätsklinikum Düsseldorf, Düsseldorf, Germany

Expression of the cellular transmembrane receptor αvβ6 integrin is essentially restricted to malignant epithelial cells in carcinomas of a broad variety of lineages, whereas it is virtually absent in normal adult tissues. Thus, it is a highly attractive target for tumor imaging and therapy. Furthermore, αvβ6 integrin plays an important role for the epithelial–mesenchymal interaction and the development of fibrosis. **Methods:** On the basis of the ^{68}Ga chelators TRAP (triazacyclononane-triphosphinate) and NODAGA, we synthesized mono-, di-, and trimeric conjugates of the αvβ6 integrin–selective peptide cyclo(FRGDLAFp(*N*Me)K) via click chemistry. These were labeled with ^{68}Ga and screened regarding their suitability for in vivo imaging of αvβ6 integrin expression by PET and ex vivo biodistribution in severe combined immunodeficiency mice bearing H2009 tumor (human lung adenocarcinoma) xenografts. For these, αvβ6 integrin expression in tumor and other tissues was determined by β6 immunohistochemistry. **Results:** Despite the multimers showing higher αvβ6 integrin affinities (23–120 pM) than the monomers (260 pM), the best results—that is, low background uptake and excellent tumor delineation—were obtained with the TRAP-based monomer ^{68}Ga-avebehexin. This compound showed the most favorable pharmacokinetics because of its high polarity (log D = –3.7) and presence of additional negative charges (carboxylates) on the chelator, promoting renal clearance. Although tumor uptake was low (0.65% ± 0.04% injected dose per gram tissue [%ID/g]), it was still higher than in all other organs except the kidneys, ranging from a maximum for the stomach (0.52 ± 0.04 %ID/g) to almost negligible for the pancreas (0.07 ± 0.01 %ID/g). A low but significant target expression in tumor, lung, and stomach was confirmed by immunohistochemistry. **Conclusion:** Because of highly sensitive PET imaging even of tissues with low αvβ6 integrin expression density, we anticipate clinical applicability of ^{68}Ga-avebehexin for imaging of αvβ6 tumors and fibrosis by PET.

Key Words: positron emission tomography; ^{68}Ga; click chemistry; preclinical imaging

J Nucl Med 2017; 58:671–677
DOI: 10.2967/jnumed.116.182824

The cellular transmembrane receptor αvβ6 integrin is 1 of 8 integrins recognizing the arginine-glycine-aspartate (RGD) peptide sequence, a structural motif mediating cellular adhesion to a variety of extracellular matrix proteins, such as vitronectin and fibronectin (*1*). In contrast to other popular RGD-binding integrins, such as $\alpha_v\beta_3$ and α5β1, which are expressed by different cell types and have gained considerable attention due to their involvement in formation and sprouting of blood and lymphatic vessels (vascularization, angiogenesis, and lymphangiogenesis) (*2*), αvβ6 integrin levels in adult tissues are generally low (*3*). Expression of αvβ6 integrin is restricted to epithelial cells (*4*), which is already pointing to a potential relevance for tumor management because most malignant neoplasms (85%) are carcinomas (*5*), that is, tumors of epithelial origin. Indeed, many carcinomas show an enhanced αvβ6 integrin expression (*6*), for example, pancreatic (*7*), cholangiocellular (*8*), gastric (*9,10*), breast (*11*), ovarian (*12,13*), colon (*14*), and those of the upper aerodigestive tract (*15*). αvβ6 integrin has furthermore been described as a marker for increased invasiveness and malignancy of several carcinomas and thus, poor prognosis (*6,9,12,14*). As such, the cancer integrin αvβ6 is an attractive target for specific tumor imaging and therapy. Beyond that, it plays an important role in the epithelial–mesenchymal interaction, for example, during development of biliary (*16*), renal (*17*), and pulmonary (*18*) fibrosis.

The occurrence and significance of αvβ6 integrin have prompted research on αvβ6-specific, nonpeptidic (*19*) and peptidic inhibitors (*20–23*). Such compounds, for example, the linear peptides A20FMDV2 (sequence: NAVPNLRGDLQVLAQKVART, derived from foot-and-mouth disease virus, FMDV) (*21*), H2009.1 (sequence: RGDLATLRQL) (*22*), and cyclic peptide $S_0$2 (*23*) were equipped with radiolabels and applied for in vivo imaging of αvβ6 expression (*24*) by SPECT (*25–27*) and PET (*21,28–32*). More recently, efforts directed at further downsizing and metabolic stabilization of FMDV peptide–derived αvβ6 integrin ligands led to discovery of the cyclic nonapeptide cyclo(FRGDLAFp(*N*Me)K) (*33*), which exhibits high αvβ6 binding affinity (0.26 nM), remarkable selectivity against other integrins ($\alpha_v\beta_3$, 632 nM; α5β1, 73 nM; αvβ5 and αIIbβ3, >1 μM), and full stability in human plasma up to 3 h. In addition, its activity was not compromised by functionalization on the lysine side chain, rendering it an optimal starting point for elaboration of molecular probes.

We aimed at the corresponding probes for application in PET imaging, labeled with ^{68}Ga (half-life, 68 min), which is conveniently available from ^{68}Ge/^{68}Ga generators (small benchtop devices acting as long-lived regenerative sources for $^{68}Ga^{III}$ in dilute HCl). For ^{68}Ga

Received Aug. 18, 2016; revision accepted Nov. 14, 2016.
For correspondence or reprints contact: Johannes Notni, Lehrstuhl für Pharmazeutische Radiochemie, Technische Universität München, Walther-Meissner-Strasse 3, D-85748 Garching, Germany.
E-mail: johannes.notni@tum.de
Published online Dec. 15, 2016.

radiolabeling, the peptide must be equipped with a chelator capable of binding the radiometal ion into a kinetically inert complex. For this purpose, we selected the chelator TRAP (*34*) (1,4,7-triazacyclononane-1,4,7-tris[methylene(2-carboxyethyl)]phosphinic acid (*35*)), because its extraordinary affinity to (*36–38*) and selectivity for (*39–41*) gallium radionuclides enables highly efficient and reliable radiolabeling procedures (*42*). Because of the presence of 3 independent sites for conjugation, TRAP allows for facile attachment of additional reporter molecules (*43*) or multimerization of targeting vectors (*44*), which is particularly conveniently done by means of click chemistry, that is, copper-catalyzed alkyne-azide cycloaddition (CuAAC) (*45*).

MATERIALS AND METHODS

Syntheses and analytic characterization of the novel compounds are described in the supplemental materials (available at http://jnm.snmjournals.org).

Integrin αvβ6 Affinities

Integrin binding assays were performed as described previously (*33*) by enzyme-linked immune sorbent assays. Briefly, 96-well plates were coated with latency-associated peptide (transforming growth factor β) as extracellular matrix protein. Free binding sites were blocked by incubation with bovine serum albumin. Solutions of the respective compounds were added, followed by a solution of the integrin. Surface-bound integrin was detected by subsequent incubation with a primary antibody (mouse-antihuman) and a second antibody-peroxidase conjugate (antimouse horseradish peroxydase). After addition of the dye tetramethylbenzidine and quenching of the reaction by addition of sulphuric acid, the absorbance signal at $\lambda = 405$ nm was measured. The determined 50% inhibition concentration value for the inhibitor is referenced to the internal standard RTD_lin (linear helical RTD-peptide RTDLDSLRT) with an αvβ6-binding affinity of 33 nM.

Radiochemistry

^{68}Ga labeling was done using an automated system (GallElut^{+}; Scintomics) as described previously (*36*). Briefly, nonprocessed eluate of a ^{68}Ge/^{68}Ga generator with SnO_2 matrix (IThemba LABS, SA; 1.25 mL, eluent: 1 M HCl, total ^{68}Ga activity 500 MBq) was adjusted to pH 2 by adding 4-(2-hydroxyethyl)-1-piperazineethanesulfonic acid buffer solution (450 μL of a 2.7 M solution, prepared from 14.4 g 4-(2-hydroxyethyl)-1-piperazineethanesulfonic acid and 12 mL water) and used for labeling of 0.5 nmol of the respective chelator conjugate for 3 min at 95°C. Purification was done by passing the reaction mixture over a C8 light solid-phase extraction cartridge (SepPak), which was purged with water (10 mL) and the product eluted with an ethanol–water mixture (1:1 by volumes, 1 mL). The purity of the radiolabeled compounds was determined by radio–thin-layer chromatography (eluents: aqueous acetate solution or citrate solution).

Cell Lines and Animal Models

All animal studies have been performed in accordance with general animal welfare regulations in Germany and the institutional guidelines for the care and use of animals. H2009 human lung adenocarcinoma cells (CRL-5911; American Type Culture Collection) were cultivated as recommended by the distributor. To establish tumor xenografts, 6- to 8-wk-old female CB17 severe combined immunodeficiency mice (Charles River) were inoculated with 10^7 H2009 cells in Matrigel (CultrexBME, type 3 PathClear; Trevigen, GENTAUR GmbH). Mice were used for biodistribution or PET studies when tumors had grown to a diameter of 6–8 mm (3–4 wk after inoculation).

Biodistribution and PET Imaging

Animals were injected with 12–15 MBq (for PET) or 5–7 MBq (for biodistribution studies) of the radiotracers under isoflurane anesthesia and subsequently allowed to wake up with access to food and water. For blockade, 60 nmol of the respective unlabeled compound was administered 10 min before tracer injection. For biodistribution, animals were sacrificed after 90 min, and organs were harvested and weighed and the activity contained therein counted in a γ-counter (Perkin-Elmer). The injected dose per gram of tissue was calculated from organ weights and counted activities, based on individually administered doses. PET was recorded under isoflurane anesthesia 60 or 75 min after injection for 20 min on a Siemens Inveon small-animal PET system. Images were reconstructed as single frames with Siemens Inveon software, using a 3-dimensional ordered-subset expectation maximum algorithm without scatter and attenuation correction.

Immunohistochemistry

For histology and immunohistochemistry, animals were sacrificed immediately after PET imaging. Tumor tissue and representative organs were fixed in 10% neutral-buffered formalin, routinely embedded in paraffin, and cut in 2-μm sections. Hematoxylin and eosin–stained sections were prepared according to standard protocols to exclude background pathology interfering with experimental results. β_6 integrin immunohistochemistry was performed as follows: after enzymatic antigen retrieval (Pronase E, 1:20 in tris-buffered saline), unspecific protein and peroxidase binding was blocked with 3% hydrogen peroxide and 3% normal goat serum (Abcam). Immunohistochemistry was performed with a Dako autostainer using an antibody against the β_6 subunit (1:50, Calbiochem, 407317). For antibody detection, biotinylated goat-antimouse secondary antibody (Medac Diagnostics, 71-00-29) was used, visualized by a streptavidine-peroxidase system (Medac Diagnostics, 71-00-38) and diaminobenzidine (Immunologic, BS04-500). Counterstaining was done using hematoxylin.

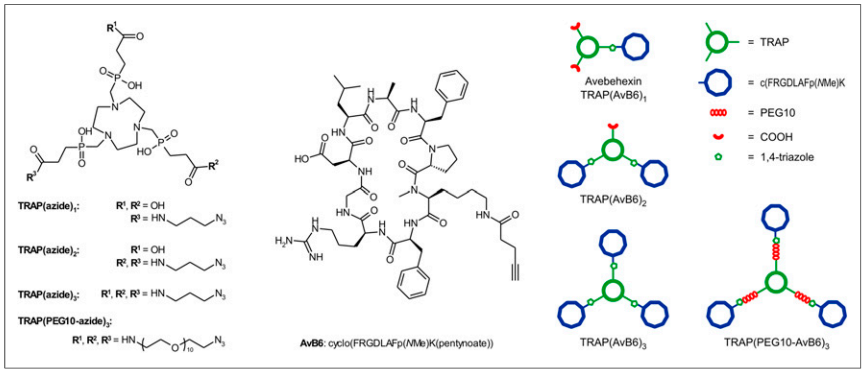

FIGURE 1. Building blocks used for synthesis of integrin αvβ6–targeted chelator conjugates by means of click chemistry (Cu-catalyzed azide-alkyne cycloaddition) and schematic overview on integrin αvβ6 addressing chelator–peptide conjugates, obtained by CuAAC reaction. Reaction conditions: $Cu(OAc)_2 \cdot H_2O$ and sodium ascorbate in H_2O/MeOH, 1 h, room temperature. Workup (Cu removal) was done at pH 2.2, using 1,4,7-triazacyclononane-1,4,7-triacetic acid (NOTA) as scavenger. Exact structural formulae are provided in supplemental materials.

RESULTS

Figure 1 shows that in combination with the previously reported TRAP(azide)$_3$ (*45*), newly synthesized TRAP derivatives with asymmetrical azide substitution pattern and

additional polyethyleneglycol (PEG) linkers represent a valuable toolkit for straightforward click-chemistry synthesis of mono-, di-, and trimeric peptide–chelator conjugates. The complementary terminal alkyne was introduced into the cyclic nonapeptide cyclo (FRGDLAFp(*N*Me)K) by amide formation with 4-pentynoic acid on the lysine side chain, resulting in the building block AvB6.

These components were used for straightforward CuAAC synthesis of 4 conjugates (Fig. 1), differing in the type of linker and the number of peptide copies (1–3) per molecule. The Cu^{II}, which is inevitably complexed by TRAP in the course of CuAAC, was subsequently removed by transchelation with 1,4,7-triazacyclononane-1,4,7-triacetic acid at pH 2.2 as described previously (*45*). In addition, functionalization of c(FRGDLAFp(*N*Me)K) with an aminohexyl linker and NODAGA (*46*), a bifunctional 1,4,7-triazacyclononane-1,4,7-triacetic acid derivative, afforded the conjugate NODAGA-AvB6 (Fig. 2), which possesses a high degree of structural similarity to the TRAP-based monomer Avebehexin. Thus, a total of 5 c(FRGDLAFp(*N*Me)K) conjugates was available for evaluation—2 monomers, 1 dimer, and 2 trimers.

αvβ6 integrin activity data shown in Table 1 confirm that functionalization of the cyclo(FRGDLAFp(*N*Me)K peptide on the lysine side chain indeed does not affect the binding affinity, because 50% inhibition concentration values of both monomers are similar to that of the nondecorated peptide (260 pM) (*33*). As expected for multimeric systems, activity is increased by a factor of approximately 2 for the dimer ^{68}Ga-TRAP(AvB6)$_2$ and by a factor of approximately 11 for the trimer ^{68}Ga-TRAP(AvB6)$_3$, relative to ^{68}Ga-avebehexin.

Exchange of the free carboxylates of TRAP by peptide substituents also had a marked influence on overall polarity. Although ^{68}Ga-avebehexin is hydrophilic (log D = –3.71), the dimer and trimer show a more lipophilic character (log D of –2.14 and –1.72, respectively; Table 1). The lipophilicity induced by the multiple peptides could only be insufficiently compensated by introduction of PEG10-linkers. ^{68}Ga-TRAP(PEG10-AvB6)$_3$ exhibited a slightly improved log D (–1.94), albeit at the expense of a decreased

TABLE 1
Octanol–Phosphate-Buffered Saline Distribution Coefficients and αvβ6 Integrin Affinities for ^{68}Ga-Labeled αvβ6 Integrin Ligands

Compound	log D	IC_{50} (pM)
^{68}Ga-NODAGA-AvB6	−2.41 ± 0.05	267 ± 31
^{68}Ga-Avebehexin	−3.71 ± 0.03	260 ± 17
^{68}Ga-TRAP(AvB6)$_2$	−2.14 ± 0.11	120 ± 23
^{68}Ga-TRAP(AvB6)$_3$	−1.72 ± 0.04	23 ± 4
^{68}Ga-TRAP(PEG10-AvB6)$_3$	−1.94 ± 0.13	87 ± 12

Affinities were determined using nonradioactive $^{69/71}Ga^{III}$ complexes.
IC_{50} = 50% inhibition concentration.

αvβ6 integrin activity (87 vs. 23 pM). A total of 30 PEG units per molecule indeed effected a lower background uptake (Fig. 3).

However, a comparison of PET images for mono-, di-, and trimeric conjugates in the same mouse, bearing a subcutaneous H2009 (human lung adenocarcinoma) αvβ6 integrin–expressing tumor (Fig. 4), shows that clearance of the PEG-trimer was still far from being optimal. ^{68}Ga-TRAP(PEG10-AvB6)$_3$ and the dimer ^{68}Ga-TRAP(AvB6)$_2$ show much higher accumulation in the abdominal region (particularly in the liver area) than the monomers ^{68}Ga-NODAGA-AvB6 and ^{68}Ga-avebehexin. A similar pattern was observed for kidney uptake and general background. Unfortunately, the higher affinities of the multimers did not effect a proportional increase of H2009 tumor accumulation, finally resulting in inferior tumor-to-organ contrast and a poor delineation of the tumor lesion (Figs. 4A and 4B). Notwithstanding this, overall polarity appears not to be the only crucial parameter, because in vivo properties of the monomers appear closely related despite their different log D values.

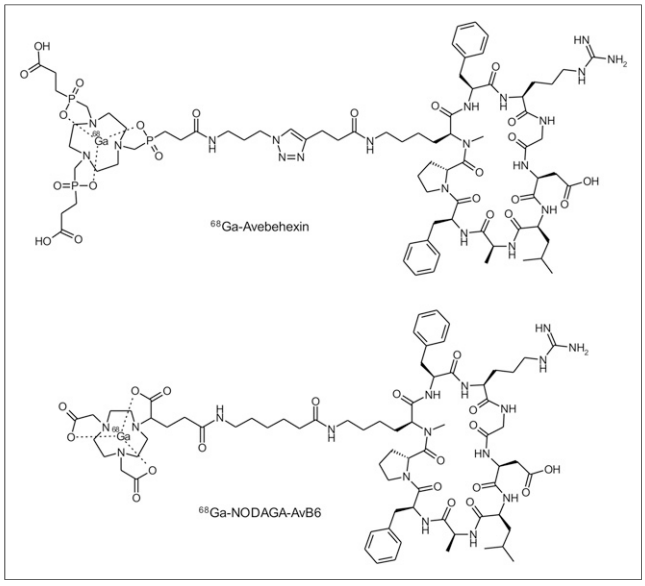

FIGURE 2. ^{68}Ga-avebehexin and ^{68}Ga-NODAGA-AvB6, 2 ^{68}Ga-labeled monomeric chelator conjugates of peptide c(FRGDLAFp(NMe)K) for in vivo mapping of integrin αvβ6 expression by PET.

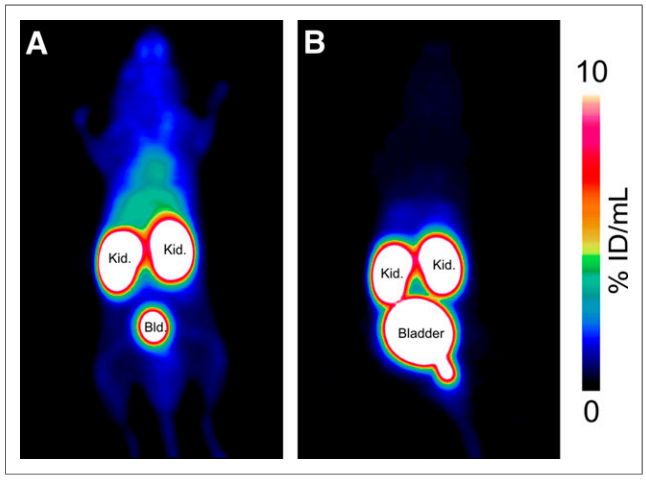

FIGURE 3. PET images (maximum-intensity projections) of severe combined immunodeficiency mice recorded 75 min after administration of 20 MBq (1 nmol, 20 MBq/nmol) of ^{68}Ga-TRAP(AvB6)$_3$ (A) and ^{68}Ga-TRAP(PEG10-AvB6)$_3$ (B), illustrating effect of PEG10 linkers in side chains on overall pharmacokinetics. Bld. = bladder; Kid. = kidneys.

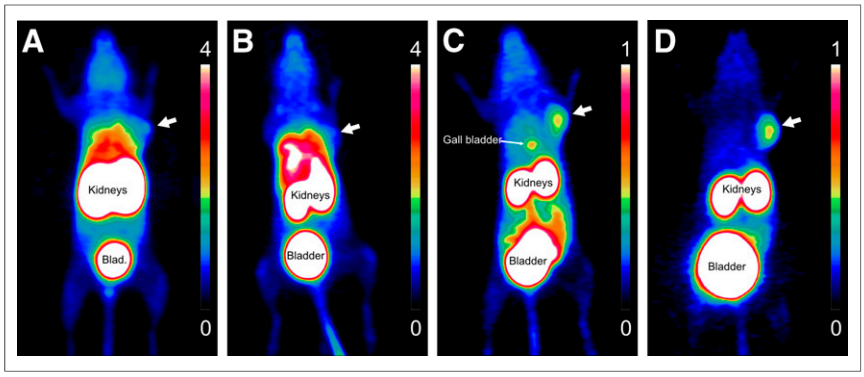

FIGURE 4. PET images (maximum-intensity projections, 75 min after injection) of severe combined immunodeficiency mouse bearing subcutaneous H2009 xenograft (human lung adenocarcinoma, position is indicated by white arrow), using approximately 15 MBq (0.3–0.4 nmol, 40–50 MBq/nmol) of ^{68}Ga-TRAP(PEG10-AvB6)$_3$ (A), ^{68}Ga-TRAP(AvB6)$_2$ (B), ^{68}Ga-NODAGA-AvB6 (C), and ^{68}Ga-avebehexin (D). Scale bars indicate percentage injected dose per mL; note the different upper limits (4 for A and B, 1 for C and D). Blad = bladder.

The PET image obtained for the hydrophilic ^{68}Ga-avebehexin (log D = –3.71, Fig. 4D) is comparable to that of ^{68}Ga-NODAGA-AvB6 (Fig. 4C), although the log D value of the latter is much closer to that of ^{68}Ga-TRAP(AvB6)$_2$ (–2.41 and –2.14, respectively).

The virtually complete lack of hepatobiliary excretion and the low background uptake rendered ^{68}Ga-avebehexin the most attractive compound for further investigation. Figure 5 confirms that the H2009 tumor is clearly delineated despite only a fraction of tumor cells that is positive for β6 integrin according to immunohistochemistry (Fig. 6), demonstrating high sensitivity of the tracer. Beyond that, it can be noticed that particularly the tumor cells adjacent to desmoplastic stroma show high β6 integrin expression in a membraneous and cytoplasmic pattern (Fig. 6B), highlighting the aforementioned link between αvβ6 integrin expression and epithelial–mesenchymal interaction.

PET and immunohistochemistry are well correlated with ex vivo biodistribution data (Fig. 7). Apart from excretion-related elevated activity levels in the kidneys and urinary bladder, the highest uptake is found in the H2009 tumor, whereas the comparably low absolute value (0.65 percentage injected dose per gram) is explained by the relatively low β6 integrin expression. Specificity is proven by a marked decrease of this signal on coinjection of excess unlabeled compound (blockade), which can be seen as well in PET (Fig. 5A). Some other blockable uptake can be explained by a low but not entirely insignificant αvβ6 integrin expression in the epithelial cells of some internal organs. For example, immunohistochemistry confirmed that β6 integrin is weakly expressed by bronchial as well as alveolar epithelial cells in the lung (Fig. 6C) and by parietal cells in the glandular part of the mouse stomach (Fig. 6D). On the other hand, the pancreatic tissue, for example, shows no β6 integrin expression in any cellular compartment (Fig. 6E), resulting comparably insignificant uptake for both control and blockade. The immunohistochemistry furthermore corresponds essentially to the human expression patterns (*7*) and suggests that similar imaging results might be obtained in humans.

DISCUSSION

To facilitate interpretation of the in vivo behavior of the investigated compounds, it needs to be emphasized that high

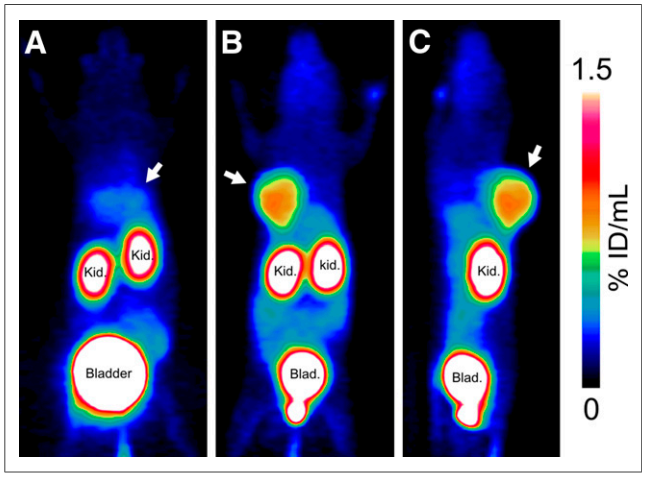

FIGURE 5. ^{68}Ga-avebehexin PET images (maximum-intensity projections, 60 min after injection) of 2 different H2009-bearing severe combined immunodeficiency mice, one with (blockade; A) and one without coinjection of 60 nmol avebehexin (control; B, dorsal view and C, sagittal view; 12 MBq, 53 pmol, 230 MBq/nmol). H2009 tumor positions are indicated by white arrows. Blad = bladder; Kid = kidneys.

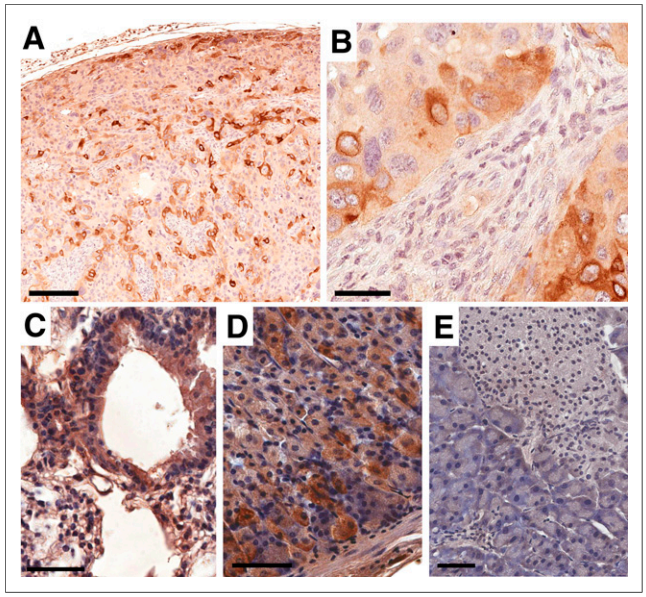

FIGURE 6. β6 integrin immunohistochemistry (IHC) of H2009 tumor (A and B), lung (C), glandular stomach (D), and pancreas (E) of same animal used for control PET scans (Figs. 5B and 5C). Bars indicate 200 μm (A) and 50 μm (B–E). Note that β6 integrin dimerizes only with αv chain, thus obviating a separate αv IHC for determination of actual αvβ6 distribution.

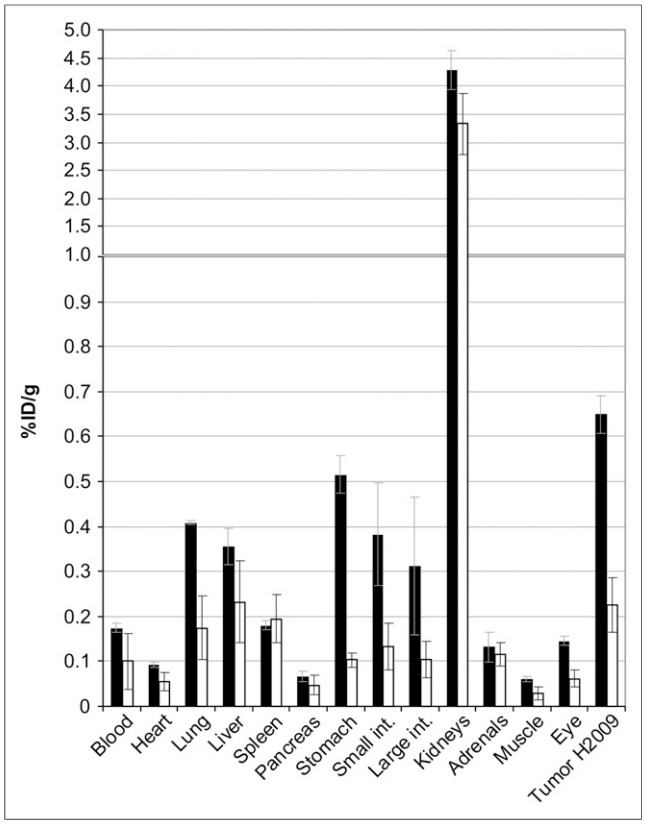

FIGURE 7. Biodistribution of approximately 12 MBq of ^{68}Ga-avebehexin in H2009 xenografted severe combined immunodeficiency mice, 90 min after injection, expressed as percentage injected dose per gram tissue; mean ± SD, $n = 4$. Black bars (control): 63 ± 10 pmol (190 ± 40 MBq/nmol); white bars (blockade): 64 ± 6 nmol (0.19 ± 0.02 MBq/nmol) (Supplemental Table 1 provides data in numeric form and tumor-to-tissue ratios).

receptor affinity is a necessary, but not sufficient, condition for excellent in vivo performance. Pharmacokinetics are largely determined by a compound's polarity and charge. A pronounced hydrophilicity promotes a fast excretion from nontarget tissues via the kidneys and the urinary tract, which is desired for imaging probes. Concerning receptor affinities, it has been shown in numerous studies that tethering multiple copies of receptor ligands, for example, $\alpha_v\beta_3$ integrin–targeting peptides of the cyclo(RGDXK) type, to a given reporter (e.g., radionuclide or fluorophor) is a reliable method to obtain constructs with increased integrin activity as well as higher uptake in $\alpha_v\beta_3$ integrin–expressing tumors (*36,47–54*). The same was observed for α5β1 integrin tracers based on a α5β1-specific pseudopeptide (*55–57*), suggesting that integrin-targeted radiopharmaceuticals might generally benefit from multimerization. Thus, it appears somewhat counterintuitive that in the present case, the best imaging results were obtained with the monomeric conjugates despite their lower αvβ6 integrin activities. We thus assume that the poor performance of the trimers is most probably a result of their lower degree of hydrophilicity; however, more detailed investigations will be necessary to substantiate this hypothesis.

The excellent clearance from nontarget tissues is the main reason why we consider ^{68}Ga-avebehexin a top choice for clinical translation. The current results are underscoring the utility of monoconjugated triazacyclononane-triphosphinate chelators with additional polar *P*-substitutents for improvement of hydrophilicity and renal clearance of ^{68}Ga radiopharmaceuticals (*58,59*). Although tumor uptake of ^{68}Ga-avebehexin was quite low because of low target expression, it was found to be higher than in all other organs, in particular, the lung, liver, stomach, and intestines (disregarding the kidneys wherein activity is concentrated because of excretion). The pronounced target specificity and a decent tumor-to-background (i.e., muscle) ratio (10.8 ± 1.3, Supplemental Table 1) raise high expectations regarding a clinical application of ^{68}Ga-avebehexin for mapping of elevated αvβ6 integrin levels in epithelial tumors by PET. Particularly in view of the previously reported high expression of αvβ6 integrin in pancreatic adenocarcinoma (*7*), the high tumor-to-pancreas ratio (9.9 ± 1.6) suggests suitability for imaging of this type of tumor. Notwithstanding this, more detailed investigations of pharmacodynamics, such as biodistribution data for more time points, will be necessary to fully define the scope and limitations for ^{68}Ga-avebehexin, which will be reported in due course.

CONCLUSION

For elaboration of tracers from targeting peptides, the fast, click-chemistry–driven synthesis of substantially different types of conjugates for biologic screening was shown to be an efficient way to identify the structural key parameters for a successful in vivo transfer. In this respect, we like to emphasize that contrary to a large body of previous work, multimerization did not work for the αvβ6 integrin–selective peptide c(FRGDLAFp(*N*Me)K). Although the multimers showed improved αvβ6 integrin affinities as expected, they did not exhibit improved target (i.e., tumor) accumulation in PET scans but instead possessed inferior pharmacokinetics compared with the respective monomers.

Because of its excellent renal clearance and the resulting low background signal, the monomeric TRAP-conjugate ^{68}Ga-avebehexin enabled highly sensitive PET imaging even of moderate αvβ6 integrin expression levels in subcutaneous H2009 (lung adenocarcinoma) xenografts in mice. It thus allows future in vivo studies on some fundamental questions of tumor biology that recently caused an increasing interest in mapping αvβ6 integrin, such as the exact role of αvβ6 integrin overexpression and integrin-mediated epithelial–mesenchymal transition during tumor invasion, metastasis, and development of resistance to chemotherapies. Furthermore, we anticipate that ^{68}Ga-avebehexin will prove clinically useful for specific PET imaging of cancers with high αvβ6 integrin expression, such as pancreatic, ovarian, lung, and gastric carcinoma as well as invasive head and neck carcinomas.

DISCLOSURE

Financial support that was provided by the Deutsche Forschungsgemeinschaft to Johannes Notni (grant #NO822/4-1 and SFB 824, project Z1) and to Katja Steiger and Wilko Weichert (by SFB 824, project Z2); by Center of Integrated Protein Science Munich, CIPSM to Horst Kessler; and by International Graduate School of Science and Engineering, IGSSE) to Tobias G. Kapp is gratefully acknowledged. No other potential conflict of interest relevant to this article was reported.

ACKNOWLEDGMENTS

We thank Markus Schwaiger for granting access to imaging devices; Sibylle Reder and Markus Mittelhäuser for assistance with animal PET; and Alexander Wurzer, Martina Wirtz, and Monika Beschorner for laboratory assistance.

REFERENCES

1. Margadant C, Monsuur HN, Norman JC, Sonnenberg A. Mechanisms of integrin activation and trafficking. *Curr Opin Cell Biol.* 2011;23:607–614.
2. Avraamides CJ, Garmy-Susini B, Varner JA. Integrins in angiogenesis and lymphangiogenesis. *Nat Rev Cancer.* 2008;8:604–617.
3. Breuss JM, Gillett N, Lu L, Sheppard D, Pytela R. Restricted distribution of integrin β6 mRNA in primate epithelial tissues. *J Histochem Cytochem.* 1993;41:1521–1527.
4. Niu G, Chen X. Why integrin as a primary target for imaging and therapy. *Theranostics.* 2011;1:30–47.
5. Krebs in Deutschland 2011/2012. GEKID website. http://www.gekid.de/Doc/krebs_in_deutschland_2015.pdf. Published August 10, 2015. Accessed March 1, 2017.
6. Bandyopadhyay A, Raghavan S. Defining the role of integrin αvβ6 in cancer. *Curr Drug Targets.* 2009;10:645–652.
7. Sipos B, Hahn D, Carceller A, et al. Immunohistochemical screening for β6-integrin subunit expression in adenocarcinomas using a novel monoclonal antibody reveals strong up-regulation in pancreatic ductal adenocarcinomas in vivo and in vitro. *Histopathology.* 2004;45:226–236.
8. Patsenker E, Wilkens L, Banz V, et al. The αvβ6 integrin is a highly specific immunohistochemical marker for cholangiocarcinoma. *J Hepatol.* 2010;52:362–369.
9. Kawashima A, Tsugawa S, Boku A, et al. Expression of αv integrin family in gastric carcinomas: increased αvβ6 is associated with lymph node metastasis. *Pathol Res Pract.* 2003;199:57–64.
10. Zhang ZY, Xu KS, Wang JS, et al. Integrin αvβ6 acts as a prognostic indicator in gastric carcinoma. *Clin Oncol.* 2008;20:61–66.
11. Arihiro K, Kaneko M, Fujii S, Inai K, Yokosaki Y. Significance of alpha 9 beta 1 and alpha v beta 6 integrin expression in breast carcinoma. *Breast Cancer.* 2000;7:19–26.
12. Ahmed N, Pansino F, Clyde R, et al. Overexpression of αvβ6 integrin in serous epithelial ovarian cancer regulates extracellular matrix degradation via the plasminogen activation cascade. *Carcinogenesis.* 2002;23:237–244.
13. Ahmed N, Riley C, Rice GE, Quinn MA, Baker S. αvβ6 integrin: a marker for the malignant potential of epithelial ovarian cancer. *J Histochem Cytochem.* 2002;50:1371–1380.
14. Bates RC, Bellovin DI, Brown C, et al. Transcriptional activation of integrin β6 during the epithelial-mesenchymal transition defines a novel prognostic indicator of aggressive colon carcinoma. *J Clin Invest.* 2005;115:339–347.
15. Ramos DM, But M, Regezi BL, et al. Expression of integrin β6 enhances invasive behavior in oral squamous cell carcinoma. *Matrix Biol.* 2002;21:297–307.
16. Wang B, Dolinski BM, Kikuchi N, et al. Role of αvβ6 integrin in acute biliary fibrosis. *Hepatology.* 2007;46:1404–1412.
17. Hahm K, Lukashev ME, Luo Y, et al. αvβ6 integrin regulates renal fibrosis and inflammation in Alport mouse. *Am J Pathol.* 2007;170:110–125.
18. Horan GS, Wood S, Ona V, et al. Partial inhibition of integrin αvβ6 prevents pulmonary fibrosis without exacerbating inflammation. *Am J Respir Crit Care Med.* 2008;177:56–65.
19. Goodman SL, Hölzemann G, Sulyok GA, Kessler H. Nanomolar small molecule inhibitors for αvβ6, αvβ5, and αvβ3 integrins. *J Med Chem.* 2002;45:1045–1051.
20. Kraft S, Diefenbach B, Mehta R, Jonczyk A, Luckenbach GA, Goodman SL. Definition of an unexpected ligand recognition motif for αvβ6 integrin. *J Biol Chem.* 1999;274:1979–1985.
21. Hausner SH, DiCara D, Marik J, Marshall JF, Sutcliffe JF. Use of a peptide derived from foot-and-mouth disease virus for the noninvasive imaging of human cancer: generation and evaluation of 4-[^{18}F]fluorobenzoyl A20FMDV2 for in vivo imaging of integrin αvβ6 expression with positron emission tomography. *Cancer Res.* 2007;67:7833–7840.
22. Li S, Mcguire MJ, Lin M, et al. Synthesis and characterization of a high-affinity αvβ6-specific ligand for in vitro and in vivo applications. *Mol Cancer Ther.* 2009;8:1239–1249.
23. Kimura RH, Teed R, Hackel BJ, et al. Pharmacokinetically stabilized cystine knot peptides that bind alpha-v-beta-6 integrin with single-digit nanomolar affinities for detection of pancreatic cancer. *Clin Cancer Res.* 2012;18:839–849.
24. Liu H, Wu Y, Wang F, Liu Z. Molecular imaging of integrin αvβ6 expression in living subjects. *Am J Nucl Med Mol Imaging.* 2014;4:333–345.
25. John AE, Luckett JC, Tatler AL, et al. Preclinical SPECT/CT imaging of αvβ6 integrins for molecular stratification of idiopathic pulmonary fibrosis. *J Nucl Med.* 2013;54:2146–2152.
26. Liu Z, Liu H, Ma T, et al. Integrin $\alpha v\beta_6$-targeted SPECT imaging for pancreatic cancer detection. *J Nucl Med.* 2014;55:989–994.
27. Zhu X, Li J, Hong Y, et al. ^{99m}Tc-labeled cystine knot peptide targeting integrin αvβ6 for tumor SPECT imaging. *Mol Pharm.* 2014;11:1208–1217.
28. Hausner SH, Abbey CK, Bold RJ, et al. Targeted in vivo imaging of integrin αvβ6 with an improved radiotracer and its relevance in a pancreatic tumor model. *Cancer Res.* 2009;69:5843–5850.
29. Singh AN, McGuire MJ, Li S, et al. Dimerization of a phage-display selected peptide for imaging of αvβ6-integrin: two approaches to the multivalent effect. *Theranostics.* 2014;4:745–760.
30. Hausner SH, Bauer N, Sutcliffe JL. In vitro and in vivo evaluation of the effects of aluminum [^{18}F]fluoride radiolabeling on an integrin αvβ6-specific peptide. *Nucl Med Biol.* 2014;41:43–50.
31. Hausner SH, Bauer N, Hu LY, Knight LM, Sutcliffe JL. The effect of bi-terminal PEGylation of an integrin αvβ6-targeted ^{18}F-peptide on pharmacokinetics and tumor uptake. *J Nucl Med.* 2015;56:784–790.
32. Hausner SH, Carpenter RD, Bauer N, Sutcliffe JL. Evaluation of an integrin αvβ6-specific peptide labeled with [^{18}F]fluorine by copper-free, strain-promoted click chemistry. *Nucl Med Biol.* 2013;40:233–239.
33. Maltsev OV, Marelli UK, Kapp TG, et al. Stable peptides instead of stapled peptides: highly potent αvβ6-selective integrin ligands. *Angew Chem Int Ed Engl.* 2016;55:1535–1539.
34. Notni J, Šimeček J, Wester HJ. Phosphinic acid functionalized polyazacycloalkane chelators for radiodiagnostics and radiotherapeutics: unique characteristics and applications. *ChemMedChem.* 2014;9:1107–1115.
35. Notni J, Hermann P, Havlíčková J, et al. A triazacyclononane-based bifunctional phosphinate ligand for the preparation of multimeric ^{68}Ga tracers for positron emission tomography. *Chem Eur J.* 2010;16:7174–7185.
36. Notni J, Šimeček J, Hermann P, Wester HJ. TRAP, a powerful and versatile framework for gallium-68 radiopharmaceuticals. *Chemistry.* 2011;17:14718–14722.
37. Šimeček J, Schulz M, Notni J, et al. Complexation of metal ions with TRAP (1,4,7-triazacyclononane-phosphinic acid) ligands and 1,4,7-triazacyclononane-1,4,7-triacetic acid: phosphinate-containing ligands as unique chelators for trivalent gallium. *Inorg Chem.* 2012;51:577–590.
38. Poty S, Désogère P, Šimeček J, et al. MA-NOTMP: A Triazacyclononane trimethylphosphinate based bifunctional chelator for gallium radiolabeling of biomolecules. *ChemMedChem.* 2015;10:1475–1479.
39. Šimeček J, Hermann P, Wester HJ, Notni J. How is ^{68}Ga-labeling of macrocyclic chelators influenced by metal ion contaminants in ^{68}Ge/^{68}Ga generator eluates? *ChemMedChem.* 2013;8:95–103.
40. Simeček J, Zemek O, Hermann P, Wester HJ, Notni J. A monoreactive bifunctional triazacyclononane-phosphinate chelator with high selectivity for Gallium-68. *ChemMedChem.* 2012;7:1375–1378.
41. Máté G, Šimeček J, Pniok M, et al. The influence of the combination of carboxylate and phosphinate pendant arms in 1,4,7-triazacyclononane-based chelators on their ^{68}Ga labeling properties. *Molecules.* 2015;20:13112–13126.
42. Notni J, Pohle K, Wester HJ. Comparative gallium-68 labeling of TRAP-, NOTA-, and DOTA-peptides: practical consequences for the future of gallium-68-PET. *EJNMMI Res.* 2012;2:28.
43. Notni J, Hermann P, Dregely I, Wester HJ. Convenient synthesis of gallium-68 labeled gadolinium(III) complexes: towards bimodal responsive probes for functional imaging with PET/MRI. *Chemistry.* 2013;19:12602–12606.
44. Notni J, Plutnar J, Wester HJ. Bone seeking TRAP conjugates: surprising observations and implications on development of gallium-68-labeled bisphosphonates. *EJNMMI Res.* 2012;2:13.
45. Baranyai Z, Reich D, Vágner A, et al. A shortcut to high-affinity Ga-68 and Cu-64 radiopharmaceuticals: one-pot click chemistry trimerisation on the TRAP platform. *Dalton Trans.* 2015;44:11137–11146.
46. Eisenwiener KP, Prata MIM, Buschmann I, et al. NODAGATOC, a new chelator-coupled somatostatin analogue labeled with [^{67}/^{68}Ga] and [^{111}In] for SPECT, PET, and targeted therapeutic applications of somatostatin receptor (hsst2) expressing tumors. *Bioconjug Chem.* 2002;13:530–541.

47. Šimeček J, Hermann P, Havlíčková J, et al. A cyclen-based tetraphosphinate chelator for preparation of radiolabeled tetrameric bioconjugates. *Chemistry.* 2013;19:7748–7757.
48. Thumshirn G, Hersel U, Goodman SL, Kessler H. Multimeric cyclic RGD peptides as potential tools for tumor targeting: solid-phase peptide synthesis and chemoselective oxime ligation. *Chem Eur J.* 2003;9:2717–2725.
49. Poethko T, Schottelius M, Thumshirn G, et al. Two-step methodology for high-yield routine radiohalogenation of peptides: ^{18}F-labeled RGD and octreotide analogs. *J Nucl Med.* 2004;45:892–902.
50. Dijkgraaf I, Kruijtzer JAW, Liu S, et al. Improved targeting of the αvβ3 integrin by multimerisation of RGD peptides. *Eur J Nucl Med Mol Imaging.* 2007;34:267–273.
51. Wängler C, Maschauer S, Prante O, et al. Multimerization of cRGD peptides by click chemistry: synthetic strategies, chemical limitations, and influence on biological properties. *ChemBioChem.* 2010;11:2168–2181.
52. Liu S. Radiolabeled Cyclic RGD peptides as integrin αvβ3-targeted radiotracers: maximizing binding affinity via bivalency. *Bioconjug Chem.* 2009;20:2199–2213.
53. Notni J, Pohle K, Wester HJ. Be spoilt for choice with radiolabeled RGD peptides: preclinical evaluation of ^{68}Ga-TRAP(RGD)$_3$. *Nucl Med Biol.* 2013;40:33–41.
54. Singh AN, Liu W, Hao G, et al. Multivalent bifunctional chelator scaffolds for gallium-68 based positron emission tomography imaging probe design: signal amplification via multivalency. *Bioconjug Chem.* 2011;22:1650–1662.
55. D'Alessandria C, Pohle K, Rechenmacher S, et al. In vivo biokinetic and metabolic characterization of the ^{68}Ga-labeled α5β1-selective peptidomimetic FR366. *Eur J Nucl Med Mol Imaging.* 2016;43:953–963.
56. Notni J, Steiger K, Hoffmann F, et al. Complementary, selective PET-Imaging of integrin subtypes α5β1 and αvβ3 using Ga-68-aquibeprin and Ga-68-avebetrin. *J Nucl Med.* 2016;57:460–466.
57. Notni J, Steiger K, Hoffmann F, et al. Variation of specific activities of Ga-68-aquibeprin and Ga-68-avebetrin enables selective PET-imaging of different expression levels of integrins α5β1 and αvβ3. *J Nucl Med.* 2016;57:1618–1624.
58. Simeček J, Zemek O, Hermann P, Notni J, Wester HJ. Tailored gallium(III) chelator NOPO: synthesis, characterization, bioconjugation, and application in preclinical PET imaging. *Mol Pharm.* 2014;11:3893–3903.
59. Simeček J, Notni J, Kapp TG, Kessler H, Wester HJ. Benefits of NOPO as chelator in gallium-68 Peptides, exemplified by preclinical characterization of ^{68}Ga-NOPO-c(RGDfK). *Mol Pharm.* 2014;11:1687–1695.

JNM The Journal of NUCLEAR MEDICINE

In Vivo PET Imaging of the Cancer Integrin αvβ6 Using ^{68}Ga-Labeled Cyclic RGD Nonapeptides

Johannes Notni, Dominik Reich, Oleg V. Maltsev, Tobias G. Kapp, Katja Steiger, Frauke Hoffmann, Irene Esposito, Wilko Weichert, Horst Kessler and Hans-Jürgen Wester

J Nucl Med. 2017;58:671-677.
Published online: December 15, 2016.
Doi: 10.2967/jnumed.116.182824

The Journal of Nuclear Medicine is published monthly.
SNMMI | Society of Nuclear Medicine and Molecular Imaging
1850 Samuel Morse Drive, Reston, VA 20190.
(Print ISSN: 0161-5505, Online ISSN: 2159-662X)

SNMMI SOCIETY OF NUCLEAR MEDICINE AND MOLECULAR IMAGING